WAVELENGTH SELECTION FOR MONOCHROMATIC AND BICHROMATIC SORTING OF FUSARIUM-DAMAGED WHEAT

S. R. Delwiche, C. S. Gaines

ABSTRACT. *Fusarium head blight (FHB) is a fungal disease that affects small cereal grains such as wheat, causing the seed to be shriveled, light in weight, and, in many circumstances, infused with the mycotoxin, deoxynivalenol (DON), a recognized human health hazard. The occurrence and severity of the disease varies with season and geographical location, with warm humid weather during flowering and the presence of crop residue from the previous year as exacerbating factors. A study was undertaken to determine the most suitable visible or near-infrared wavelengths that could be used in high-speed sorting for removal of FHB-infected soft red winter wheat kernels. Four thousand eight hundred kernels, equally divided between normal and scab-damaged conditions, from 100 commercial varieties were individually scanned in the extended visible (410 to 865 nm) and near-infrared (1031 to 1674 nm) regions. Single- and all combinations of two-wavelength linear discriminant analysis models were developed and characterized through cross-validation by the average correctness of classification percentages. Short visible (~420 nm) and moderate near-infrared (1450 to 1500 nm) wavelengths produced the highest single-term classification accuracies (at approximately 77% and 83%, respectively). The best two-term models occurred near the wavelengths of 500 and 550 nm for the visible region alone (94% accuracy), 1152 and 1248 nm for the near-infrared region alone (97%), and 750 and 1476 nm for the hybrid region (86%). Such wavelengths are, therefore, considered of importance in the design of monochromatic and bichromatic high-speed sorters for scab-damage reduction.*

Keywords. *Wheat, Fungi, Near-Infrared, Grading, Scab, Spectroscopy,* Fusarium

Fusarium head blight (FHB), also known as scab, is a fungal disease that affects small grains, which, despite the volume of research it has received since the late 1800s (Stack, 2003), is still very prevalent in the wheat of North America and elsewhere. It is predominantly spread by the asexual reproduction of the fungus *Fusarium graminearum*. Intensified by warm humid conditions during the time of flowering, the severity of FHB changes from year to year and location to location. Recent outbreaks in North America include those in the early 1980s, the mid-1990s, especially the Midwest in 1996 (Hart, 1998), and most recent, the 2003 and 2004 seasons in the soft red winter growing regions of the Eastern United States. Deleterious effects of FHB include lower yields due to loss during mechanized harvesting (Bai and Shaner, 1994), low test weight (Cunfer, 1987), and diminished baking characteristics (Dexter et al., 1996). Extensive information on the physiology and epidemiology of this fungus and its control is contained in a recently published monograph (Leonard and Bushnell, 2003).

Article was submitted for review in September 2004; approved for publication by Food & Process Engineering Institute Division of ASAE in February 2005.

Mention of trade names or commercial products is solely for the purpose of providing specific information and does not imply endorsement or recommendation by the USDA.

The authors are **Stephen R. Delwiche,** USDA/ARS, Beltsville Agricultural Research Center, Instrumentation and Sensing Laboratory, Beltsville, Maryland; and **Charles S. Gaines,** USDA/ARS, Soft Wheat Quality Laboratory, Wooster, Ohio. **Corresponding author:** Stephen R. Delwiche, USDA/ARS, Beltsville Agricultural Research Center, Instrumentation and Sensing Laboratory, Building 303, BARC-East, Beltsville, MD 20705-2350; phone: 301-504-8450; fax: 301-504-9466; e-mail: delwiche@ba.ars.usda.gov.

Often accompanying the fungus is its secondary metabolite, deoxynivalenol (DON), a tricothecene mycotoxin. Although not considered the level of health risk of other mycotoxins such as aflatoxin, DON is particularly problematic to non-ruminant animals and can cause sickness in humans. DON levels are overseen by the U.S. Food and Drug Administration through advisory limits that vary depending on the intended use of the grain. Wheat that is destined for human consumption has an advisory level of 1.0 ppm in finished products, while higher limits are allowed for swine (5 ppm) and cattle or chickens (10 ppm). A general rule of thumb for milling operations that process wheat for human consumption is that the milling procedure itself, through its separation of pericarp from the endosperm, can reduce the level of DON by half, thus making it possible for mills to process wheat with incoming levels of 2 ppm or less. However, this one-half reduction is not always realized, especially in circumstances of heavy infestation when the penetration of the fungus extends into the endosperm, as with the 2003-year crop of soft red winter wheat in the mid-Atlantic region of the United States. Further, DON concentrations in raw wheat may exceed 2 ppm and thereby preclude the ability to reduce the contaminant level to safe conditions by processing. Traditionally, grain handlers and processors of scab-damaged grain are left with just a few options: sell the downgraded lot as animal feed at a sharp discount, blend it with clean wheat to reduce the concentration of the contaminant, or attempt to remove the damaged kernels by mechanical operations and aspiration. Conventional cleaning operations in a commercial setting are not particularly effective in lowering DON (Seitz et al., 1986).

Because of a typical whitish to pinkish discoloration of the kernel and its tombstone appearance, several researchers have studied the optical characteristics of scab-infected

wheat, either by near-infrared (near-IR) reflectance spectroscopy (Dowell et al., 1999) or by digital image analysis (Ruan et al., 1998; Luo et al., 1999). Use of near-IR for estimation of DON concentration in contaminated wheat has been the focus of other recent works (Williams, 1997; Pettersson and Åberg, 2003). In an author's laboratory, feasibility of using near-IR reflectance to distinguish wheat kernels with FHB has been examined (Delwiche, 2003; Delwiche and Hareland, 2004). These studies have demonstrated that with hard red spring wheat, classification accuracies averaging 95% to 97% are possible with absorption readings at two wavelengths. The current study's purpose is to extend these findings to soft red winter wheat. Further, the results of this study are intended to be a precursor to the application of high-speed optical sorters, which are based on one or two wavelengths. This type of technology with application toward wheat has been reported for the separation of red vs. white kernels (Pasikatan and Dowell, 2003), low vs. high protein kernels (Pasikatan and Dowell, 2004), and kernels with Karnal bunt (Dowell et al., 2002). Because commercial sorters that are reliant on two wavelengths (commonly called bichromatic sorters) are typically restricted to utilizing a wavelength in the visible region and the other wavelength in the near-IR region, this study is an expansion of our previous studies by including visible (by a separate detector) as well as near-IR spectral data.

Materials and Methods

Wheat

One hundred commercial varieties (public and private releases) of soft red winter wheat (99 samples) and hard red winter wheat (one sample, a field check) were drawn from the USDA ARS Soft Wheat Quality Laboratory annual grow out program. Approximately half these varieties are presently in production, with each representing a substantial portion of the soft wheat acreage in its growing region in the eastern United States. Each sample received light cleaning and aspiration for removal of small and broken kernels, stalks, nonwheat seeds, and other foreign material.

Equipment

Two spectrometers were used. The first spectrometer, a Zeiss MCS511 (Jena, Germany) 128-element diode array unit, operating with an InGaAs detector (943.3-to-1704.6 nm), has been described elsewhere (Delwiche, 2003). The internal light source was replaced by an illumination assembly, which consisted of two externally controlled 5-V, 150-mA tungsten filament lamps with gold-coated parabolic reflectors diametrically oriented at 45° with respect to the horizontal surface, each approximately 8 mm from the nearest point of the wheat kernel. Reflected energy was captured by a low-OH fused silica single strand optical fiber (1 m length × 600 μm diameter) whose end was positioned directly above the kernel at a distance of approximately 8 mm (~6-mm diameter viewing area). A dark current scan was made with the fiber mechanically blocked. Sintered polytetrafluoroethylene (Spectralon, Labsphere, Inc., Sutton N.H.) was used as a 100% reflectance reference. The integration time was 6.8 ms per scan, and the number of co-adds was set to 32, whereupon the spectrum was transformed to $\log(1/R)$ and stored to computer file. Linear interpolation was used to transform each spectrum to a uniform wavelength spacing of 6 nm. Low sensitivity at wavelengths less than 1000 nm resulted in limiting the region of analysis to 1002 to 1704 nm. Hereafter, this region is termed the near-IR region.

The second spectrometer was used to capture reflectance readings in the visible and low wavelength region of the near infrared. A Control Development (South Bend, Ind.) 512-element silicon photodiode array spectrometer (Model PDA-512-USB) collected, interpolated, and stored reflectance readings (1-nm wavelength increment) from 380 to 899 nm, hereafter termed the extended visible region. The same illumination assembly was used, though the gold-coated reflectors were replaced with polished aluminum to improve the response in the <500-nm region. Similarly, a single strand silica fiber (1 m × 400 μm, ~4-mm diameter viewing area) captured reflected radiation. Dark current and reference scans were collected in the same manner as the first spectrometer. The integration time was 170 ms and 25 co-adds were averaged to form a spectrum.

As previously described (Delwiche, 2003), a computer-controlled two-axis movable stage (Model MAXY4009W1-S4, Velmex, Bloomfield, N.Y.) was fitted with a sheet of Bakelite that had a 7 × 7 array of milled slots for which, at a uniform time interval, each slot containing a kernel was aligned with the overlying stationary illumination assembly. Scanning of each kernel was performed while the stage was at rest. The stage's movement was preprogrammed to sequentially align each slot with respect to the illumination assembly. Kernels were placed in their slots in random orientation, though always with the main axis of each kernel coincident with the axis of the slot. Our previous work demonstrated a spectral insensitivity to kernel alignment (i.e., crease-up, -down, or -sideways) (Delwiche, 2003).

Procedure

Twenty-four scab-damaged kernels and an equal number of kernels of normal appearance were manually selected from each nursery sample. The basis for selection was primarily by kernel surface texture in combination, though to a smaller role, with kernel color, both by human visual analysis. Scab-damaged kernels are typified by a shriveled appearance and faded, chalky or pinkish tint (Atanasoff, 1920; Pugh et al., 1933). The reliance on texture over color was made for the purpose of reducing the chance of including weathered or bleached kernels in the scab-damaged category. Kernels were scanned and weighed (0.01-mg precision) while at room ambient conditions (~20°C, 50% rh). Dark current and reference scans, each manually performed, preceded the cycle of each sample's 48 kernels.

Repeatability

Six normal and six scab-damaged kernels from one sample were arbitrarily selected for repeated spectral measurement. Kernels from this sample were repeatedly loaded, scanned, and removed a total of five times. The spectra were subsequently applied to the best-performing classification models as a means of gauging model consistency as a function of a normal level of variation caused by kernel orientation during mechanical operations.

Classification Modeling

Previous research on hard red spring wheat scanned in the 1000- to 1700-nm region indicated that accurate classification (~95%) is possible with as few as two wavelengths (Delwiche, 2003; Delwiche and Hareland, 2004). Therefore, the current study placed an emphasis on no more than two wavelengths as input to discriminant functions. Linear discriminant analysis, with a squared distance metric for the discriminant function, utilized a pooled (across category) covariance matrix. Spectral preprocessing consisted of smoothing each region by convolution with a 60-nm wide (= 11-point and 61-point overlapping windows for the near-IR and visible spectrometers, respectively) Gaussian function of size (full width at half maximum) = 20 nm, and then discarding 30 nm on each end of each spectral region. The purpose of the convolution was the opposite of conventional spectroscopic analysis, which attempts to mathematically remove the effect of the instrument resolution (i.e., slit) function (Jansson, 1984). Rather, convolution was performed to establish spectral conditions similar to those of interference filters, which typically have passbands of this size. Because of the lack of sharp, measurable absorption bands in the extended visible region, the number of wavelengths in this region was reduced by selecting every 5th point for the purpose of reducing computation time. Effectively, the extended visible and near-IR regions became 410 to 865 nm [92 log(1/*R*) values] and 1032 to 1674 nm [108 log(1/*R*) values], respectively. All two-wavelength combinations were used to develop classification models, first within a detector region, and eventually in combination of both regions, whereby a wavelength was selected from each region to form the combined pair. Convolution and reduction routines were developed, and discriminant analysis (Proc Discrim - SAS, 1988) was implemented, all in the SAS macro language-programming environment (Burlew, 2001). Model accuracy was assessed by the two-category (e.g., normal, scab-damaged) average of the percentage of correctly classified kernels, in which each kernel was classified using leave-one-out cross-validation (ASTM, 2000).

Results and Discussion

Scab-damaged kernel masses (mean = 16.2 mg, *s* = 6.1 mg) were generally less than normal kernels (mean = 38.3 mg, *s* = 6.4 mg), as shown in the histograms of figure 1. The overlapping (dark shaded) region accounted for 4.6% of the total number of kernels, with 27±1 mg being the weight possessing approximately equal proportions of scab-damaged and normal kernels. Unless accomplished by aspiration or by use of a specific gravity table (Dexter et al., 1991; Tkachuk et al., 1991), sorting by mass is probably not amenable to high-speed operations. Therefore, it is desired to use an optical method for sorting that is capable of operation at high speed.

The spectral responses over the extended visible region (410 to 870 nm) are shown as mean spectra for the normal and scab-damaged categories (fig. 2). Included in this graph are ±1 standard deviation envelopes. Even at the low wavelength region, where the mean traces are most divergent, the kernel-to-kernel spectral variation within a category is sufficiently great to preclude a perfect classification for a one-wavelength model. A similar series of traces for the near-IR region is shown in figure 3. From this graph, it is seen that scab-damaged kernels had the tendency to have lower

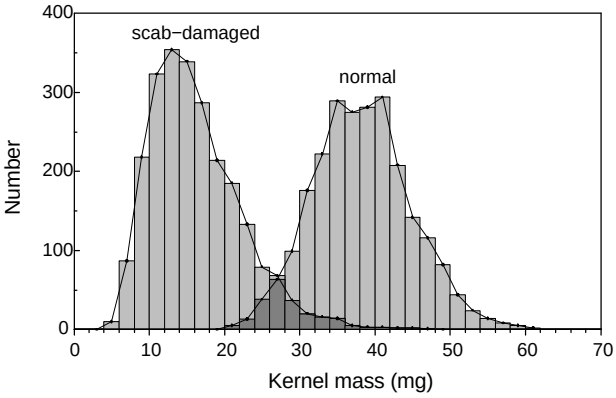

Figure 1. Histograms of masses of kernels examined in study (*n* = 2400 for each category: scab-damaged and normal).

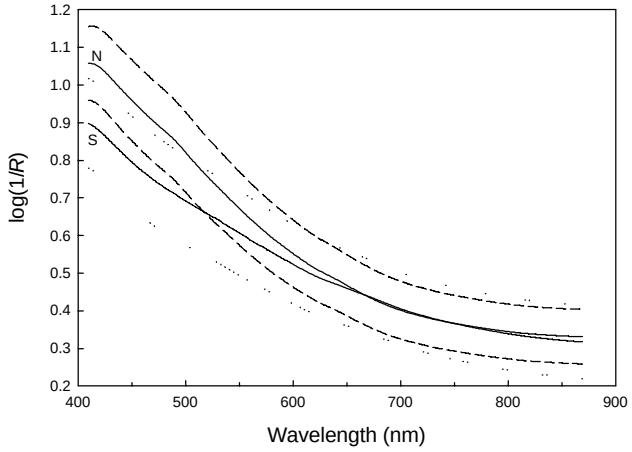

Figure 2. Mean single kernel absorption spectra (extended visible region) of normal (N, *n* = 2400) and scab-damaged (S, *n* = 2400) kernels. Also included are the ± 1 standard deviation envelopes (dashed line for normal, dotted line for scab-damaged).

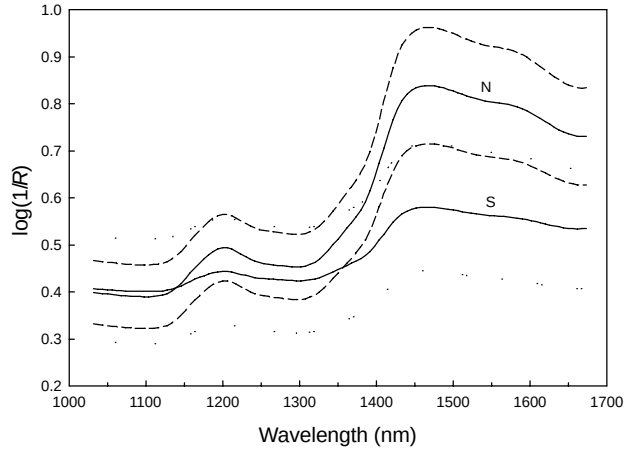

Figure 3. Mean single kernel absorption spectra (near-IR region) of normal (N, *n* = 2400) and scab-damaged (S, *n* = 2400) kernels. Also included are the ± 1 standard deviation envelopes (dashed line for normal, dotted line for scab-damaged).

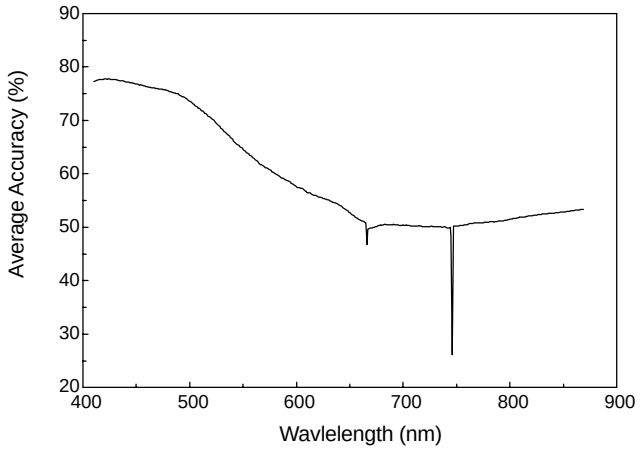

Figure 4. Average classification accuracy of single wavelength linear discriminant analysis models as a function of wavelength (extended visible region).

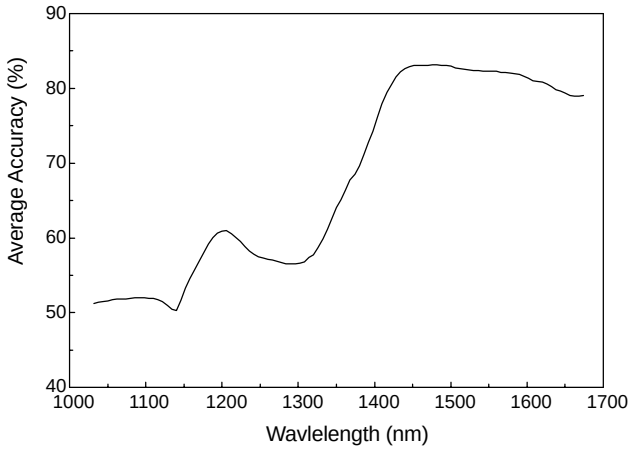

Figure 5. Average classification accuracy of single wavelength linear discriminant analysis models as a function of wavelength (near-IR region).

absorbance, but also had a greater degree of spectral variation. Single-term classification models for this wavelength region are also not capable of perfect classification, as demonstrated by the overlap in standard deviation envelopes. The degree of accuracy for single-term models as a function of wavelength is shown in figures 4 and 5, which correspond to the extended visible and near-IR regions, respectively. For the extended visible region, the lowest wavelengths, particularly those between 410 and 420 nm, produced the highest classification accuracy, with an average of approximately 77%. The downward spikes at 664 and 724 nm correspond to spectral regions of identical absorption values between scab-damaged and normal kernels. Single-wavelength model accuracy in the near-IR region (fig. 5) was highest between 1450 and 1460 nm, with an average accuracy approaching 83%.

With incorporation of a second wavelength to the extended visible region, classification accuracy improved to as high as 94.5%, as seen from the contour plot of average accuracies when one wavelength was paired with a second wavelength (fig. 6). A line of symmetry coincides with the

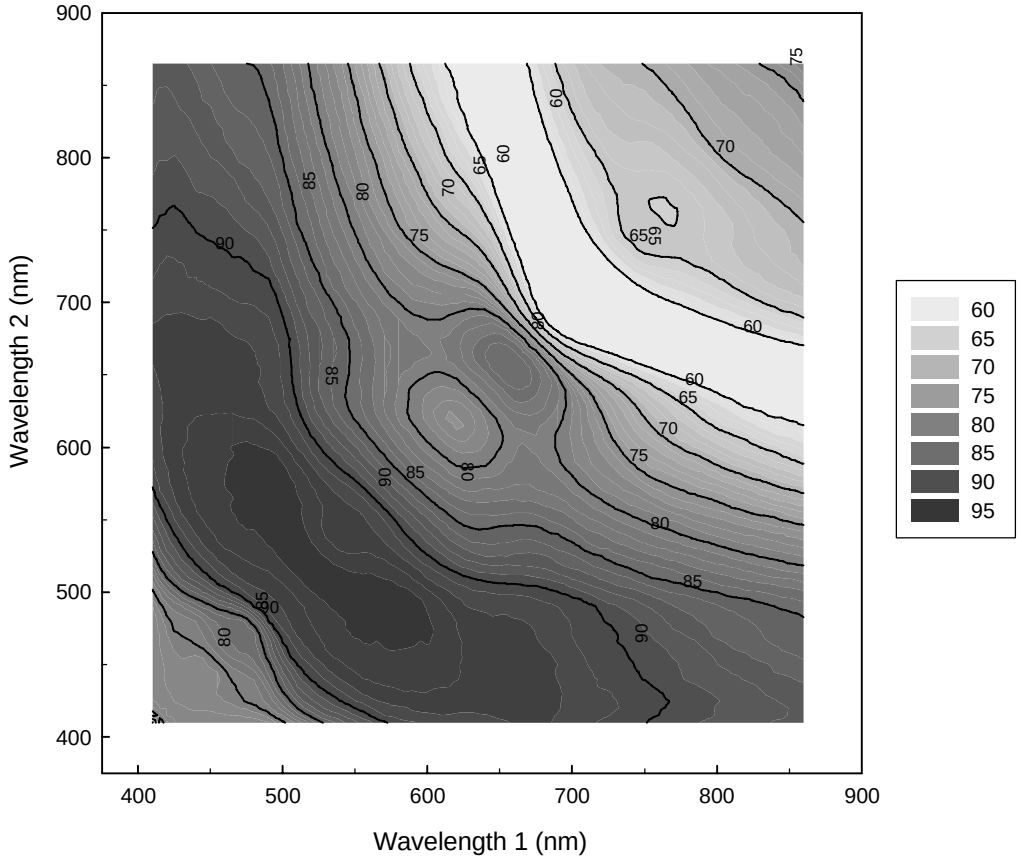

Figure 6. Contour plot of average classification accuracies of dual wavelength linear discriminant analysis models, based on extended visible region alone.

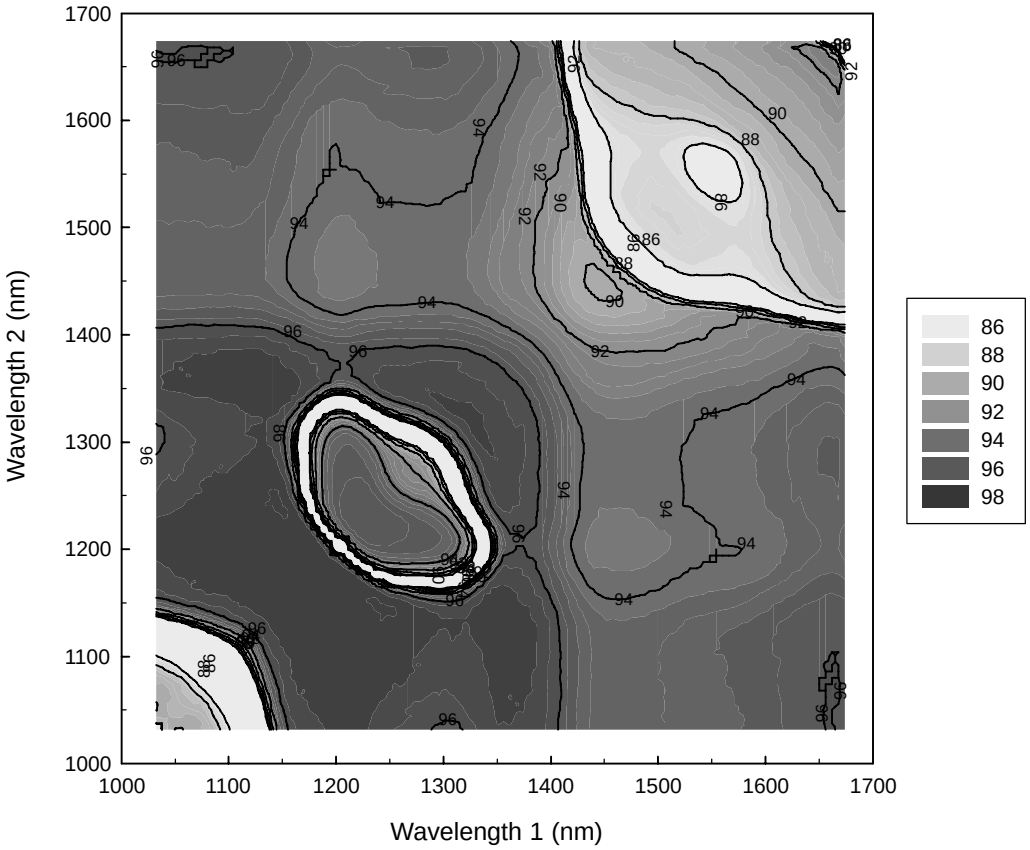

Figure 7. Contour plot of average classification accuracies of dual wavelength linear discriminant analysis models, based on near-IR region alone.

lower-left-to-upper-right diagonal. Classification accuracy was consistently high when one wavelength ranged 550 and 600 nm, and the other between 460 and 510 nm. Collectively, these regions correspond to the greatest differences in slope between normal and scab-damaged categories (fig. 2). Wavelength pairs between 700 and 800 nm demonstrated poor classification (<60% average) in this region, most likely because of the similarity in absorption of the two categories. A similar plot of the near-IR region yielded wavelength pairs with accuracies as high as 97.1% (fig. 7). This degree of accuracy was attained with wavelengths generally between 1150 and 1250 nm, which cover the broad carbohydrate

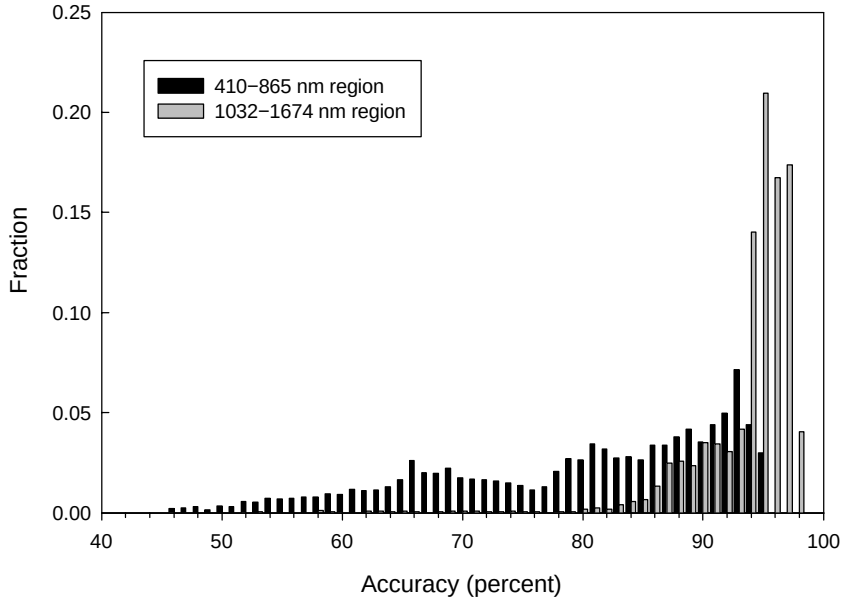

Figure 8. Distributions of average classification accuracies of the dual wavelength, single sensor LDA models for both extended visible (410-865 nm, 4186 pairs) and Near-IR (1032-1674 nm, 5778 pairs) regions. For each region, Σ *fractions* = 1.

absorption band whose peak is at approximately 1200 nm (fig. 3). This region has been previously identified for its value in sorting potential for mold-damaged wheat (Delwiche and Hareland, 2004) and corn (Pearson et al., 2004). On the whole, the near-IR region was better able to classify scab-damaged and normal kernels than the extended visible region, as shown by the distributions of their average cross-validation accuracies (fig. 8). Whereas the extended visible region produced no averages in excess of 95%, more than half of the classification models from the near-IR region were above this value.

With the restriction that wavelength pairs have to be formed by contributions from both detector regions, classification accuracy is greatest between 650 and 850 nm for the extended visible region and between 1450 and 1600 nm for the near-IR region (fig. 9). With the best average accuracies at 86.4%, the dual detector, two-wavelength classification model is not as accurate as similar models that used both wavelengths from the same detector. This is not surprising, considering that the hybrid model not only used two detectors but two spectrometers that were not standardized with respect to each other, and that these instruments scanned the kernels at different times, with slight differences in kernel orientation caused by separate manual loading. A summary of classification accuracies for some of the best one- and two-wavelength models is shown in table 1. Whereas single-wavelength models tended to classify a higher percentage of normal kernels correctly, compared to scab-damaged kernels, the opposite occurred for dual wavelength models. However, the difference between the classification accuracies of the categories did not exceed 5%.

Repeatability of Wavelength Difference Model

Repeatability results are shown in figures 10 and 11 for the extended visible and near-IR regions, respectively. The wavelengths identified in table 1, namely 500 and 550 nm for the extended visible region and 1152 and 1248 nm for the near-IR region, were used as representative of the best pairs from their respective region. Considering the extended visible region model first, when the classification model was

Table 1. Average classification accuracies for various discriminant analysis models.

		Portion Correctly Classified		
Model	Wavelengths (nm)	Normal (%)	Scab (%)	Avg. (%)
Single, extended visible region[a]	420	80.3	75.2	77.5
Single, near−IR region[b]	1476	84.1	82.2	83.1
Dual, extended visible region	500, 550	92.5	96.3	94.4
Dual, near−IR region	1152, 1248	96.4	97.8	97.1
Dual, combined regions	750, 1476	85.5	87.4	86.4

[a] 410 to 865 nm, as measured by a silicon photodiode array spectrometer.
[b] 1032 to 1674 nm as measured by an InGaAs diode array spectrometer.

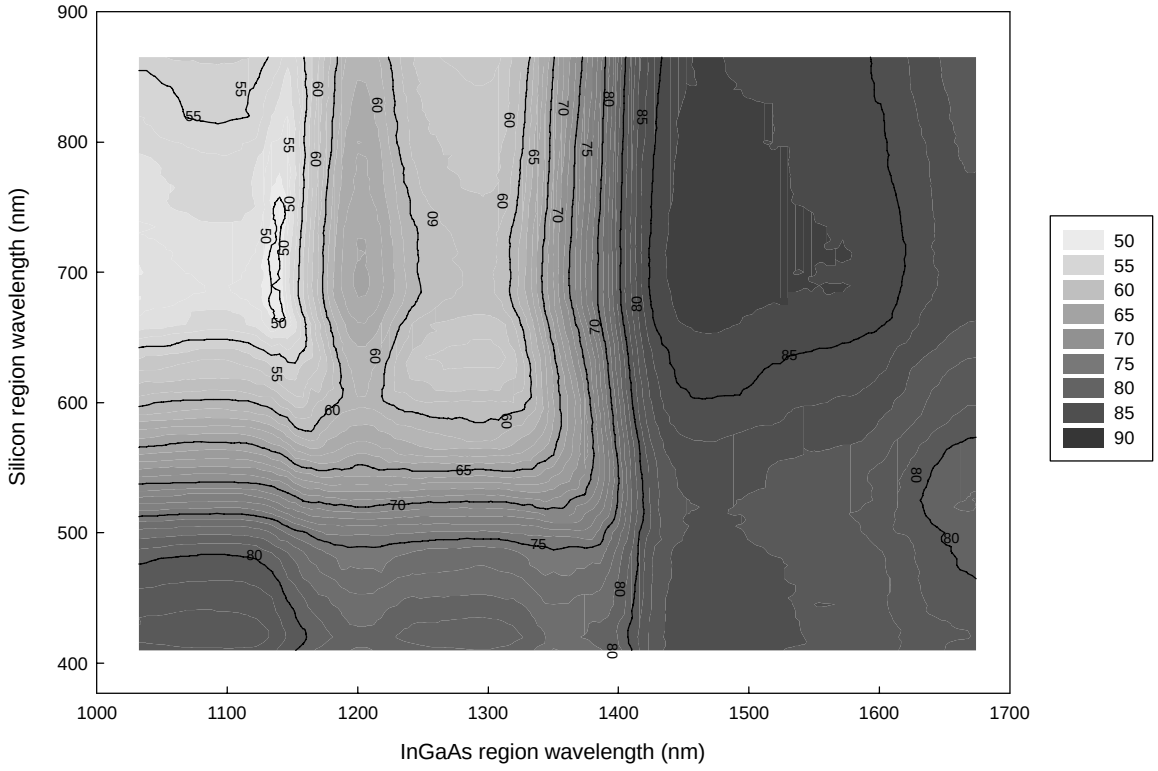

Figure 9. Contour plot of average classification accuracies of dual wavelength linear discriminant analysis models, with each sensor region contributing one wavelength.

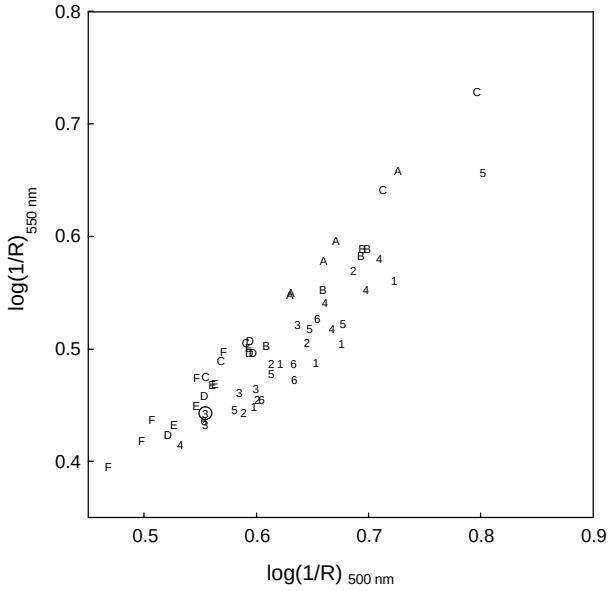

Figure 10. Absorption values of repeatability set kernels evaluated at two wavelengths (500 and 550 nm) that, in combination, produced high cross-validation accuracy (see fig. 6). Six normal (symbols 1-6) and six scab-damaged (symbols A-F) were repeatedly scanned five times each, with kernel removal and reinstatement between scans. Circled symbol corresponds to a misclassification by an existing linear discriminant analysis model that was based on these two wavelengths.

applied to the repeatability spectra (six normal kernels and six scab-damaged kernels, each scanned and reset five times), only one scan of 60 was misclassified (fig. 10). This scan belonged to a normal kernel. Likewise, equivalent results were obtained when the near-IR region model was applied to its repeatability spectra (fig. 11), though the misclassified scan was associated with a different normal kernel. Apparent from either graph is the relatively wide

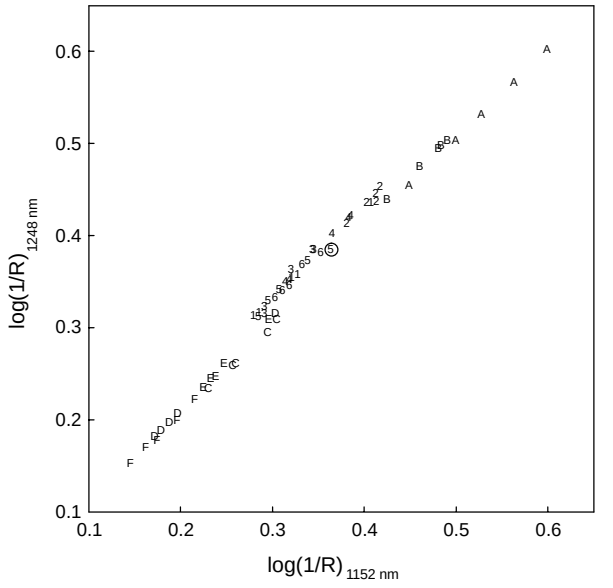

Figure 11. Absorption values of repeatability set kernels evaluated at two wavelengths (1152 and 1248 nm) that, in combination, produced high cross-validation accuracy (see fig. 7). Six normal (symbols 1-6) and six scab-damaged (symbols A-F) were repeatedly scanned five times each, with kernel removal and reinstatement between scans. Circled symbol corresponds to a misclassification by an existing linear discriminant analysis model that was based on these two wavelengths.

variation in spectral absorption of a single kernel at the chosen wavelength; however, when this wavelength is combined with the second wavelength to form the discriminant function, the function is generally sufficient for classification.

Summary and Conclusions

This study has determined that it is possible to distinguish *Fusarium*-damaged soft red winter wheat kernels by visible or near-infrared reflectance at two wavelengths. The accuracy of classification depends on the wavelength region (extended visible by silicon detector at 410 to 865 nm, near-IR by InGaAs detector at 1032 to 1674 nm) and the wavelengths selected within each region. Exhaustive searches were performed for the single best wavelength from each region, the best pair of wavelengths from each region, and the best combination of a wavelength from each region, all with the application of linear discriminant analysis. Single wavelengths at their best were capable of achieving 77% to 83% classification accuracy, whereas wavelength pairs achieved 86% to 97% accuracy. Such levels of accuracy indicate that high-speed optical sorting of wheat for scab damage should be possible.

Acknowledgements

The authors wish to thank B. Stetzler (ARS, Beltsville) for spectral data collection.

References

ASTM. 2000. E 1655. Standard practices for infrared multivariate quantitative analysis. West Conshohocken, Pa.: American Society for Testing and Materials.

Atanasoff, D. 1920. Fusarium-blight (scab) of wheat and other cereals. *J. Agr. Res* . 20(1): 1-32.

Bai, G-H., and G. Shaner. 1994. Scab of wheat: Prospects for control. *Plant Dis.* 78(8): 760-766.

Burlew, M. M. 2001. *SAS Macro Programming Made Easy* . Cary, N.C.: SAS Institute, Inc.

Cunfer, B. M. 1987. Bacterial and fungal blights of the foliage and heads of wheat. In *Wheat and Wheat Improvement,* 2nd Ed. , ed. E. G. Heyne, 528-541. Madison, Wis.: American Society of Agronomy.

Delwiche, S. R. 2003. Classification of scab- and other mold-damaged wheat kernels by near-infrared reflectance spectroscopy. *Transactions of the ASAE* 46(3):731-738.

Delwiche, S. R., and G. A. Hareland. 2004. Detection of scab damaged hard red spring wheat kernels by near-infrared reflectance. *Cereal Chem.* 81(5): 643-649.

Dexter, J. E., R. Tkachuk, and K. H. Tipples. 1991. Physical properties and processing quality of durum wheat fractions recovered from a specific gravity table. *Cereal Chem.* 68(4): 401-405.

Dexter, J. E., R. M. Clear, and K. R. Preston. 1996. Fusarium head blight: Effect on the milling and baking of some Canadian wheats. *Cereal Chem.* 73(6): 695-701.

Dowell, F. E., M. S. Ram, and L. M. Seitz. 1999. Predicting scab, vomitoxin, and ergosterol in single wheat kernels using near-infrared spectroscopy. *Cereal Chem.* 76(4): 573-576.

Dowell, F. E., T. N. Boratynski, R. E. Ykema, A. K. Dowdy, and R. T. Staten. 2002. Use of optical sorting to detect karnal bunt-infected wheat kernels. ASAE Paper No. 023007. St. Joseph, Mich.: ASAE.

Hart, L. P. 1998. Variability of vomitoxin in truckloads of wheat in a wheat scab epidemic year. *Plant Disease* 82(6): 625-630.
Jansson, P. A. 1984. *Deconvolution: With Applications in Spectroscopy.* Orlando, Fla.: Academic Press.
Leonard, K. J., and W. Bushnell. 2003. *Fusarium Head Blight of Wheat and Barley.* St. Paul, Minn.: American Phytopathological Society.
Luo, X., D. S. Jayas, and S. J. Symons. 1999. Identification of damaged kernels in wheat using a colour machine vision system. *J. Cereal Sci.* 30(1): 49-59.
Pasikatan, M. C., and F. E. Dowell. 2003. Evaluation of a high-speed color sorter for segregation of red and white wheat. *Applied Engineering in Agriculture* 19(1): 33-38.
Pasikatan, M. C., and F. E. Dowell. 2004. High-speed NIR segregation of high- and low-protein single wheat seeds. *Cereal Chem.* 81(1): 145-150.
Pearson, T. C., D. T. Wicklow, and M. C. Pasikatan. 2004. Reduction of aflatoxin and fumonisin contamination in yellow corn by high-speed dual wavelength sorting. *Cereal Chem.* 81(4): 490-498.
Pettersson, H. and L. Åberg. 2003. Near infrared spectroscopy for determination of mycotoxins in cereals. *Food Control* 14(4): 229-232.
Pugh, G. W., H. Johann, and J. G. Dickson. 1933. Factors affecting infection of wheat heads by *Gibberella saubinettii. J. Agr. Res.* 46(9): 771-797.
Ruan, R., S. Ning, A. Song, A. Ning, R. Jones, and P. Chen. 1998. Estimation of *Fusarium* scab in wheat using machine vision and a neural network. *Cereal Chem.* 75(4): 455-459.
SAS. 1988. *SAS/STAT User's Guide*, Release 6.03. Cary, N.C.: SAS Institute, Inc.
Seitz, L. M., W. D. Eustace, H. E. Mohr, M. D. Shogren, and W. T. Yamazaki. 1986. Cleaning, milling, and baking tests with hard red winter wheat containing deoxynivalenol. *Cereal Chem.* 63(2): 146-150.
Stack, R. W. 2003. History of Fusarium head blight with emphasis on North America. In *Fusarium Head Blight of Wheat and Barley*, eds. K. J. Leonard and W. R. Bushnell, 1-34. St. Paul, Minn.: The American Phytopathological Society.
Tkachuk, R., J. E. Dexter, K. H. Tipples, and T. W. Nowicki. 1991. Removal by specific gravity table of tombstone kernels and associated trichothecenes from wheat infected with Fusarium head blight. *Cereal Chem.* 68(4): 428-431.
Williams, P. C. 1997. Recent advances in near-infrared applications for the agriculture and food industries. In *Proc. of the International Wheat Quality Conference*, eds. J. L. Steele and O. K. Chung, 109-128. Manhattan, Kans.: Grain Industry Alliance.